Calibration Report of the FGM Measurements in the Cluster Active Archive (CAA)

C. Carr, P. Brown, L.-N. Alconcel, T. Oddy, P. Fox

Contents

1. Introduction

This document is the Calibration Report for the FGM (Fluxgate Magnetometer) measurements in the Cluster Active Archive (CAA). It provides the results and current status of the FGM calibration and cross calibration activities undertaken so far.

Preparation of the FGM CAA datasets spanning the operational years of the Cluster mission (2001 up the present day 2014) is a time intensive activity requiring significant manpower and computing resources. One of the reasons for this is the extensive set of analyses required to calibrate DC-magnetometer data in flight - the relatively large number and unpredictable nature of fluxgate calibration parameters do not lend themselves to purely automated calibration schemes. Another reason is the nature of the very large data volumes produced by the four Cluster FGM instruments which for the vast majority of the mission have been operational each and every orbit. Cluster is the first space mission to feature such multiple magnetometers with datasets that are comprehensive and well calibrated.

Until recently, the large processing and interpretative analysis overhead associated with multiple magnetometer calibration means that effort concentrated on producing well calibrated data sets according to the CAA schedule, as opposed to investigating trends in the long term drift of the FGM calibration parameters. The FGM CAA data generation has caught up with that of the real-time mission, so long term trending and statistical analysis of the FGM calibration parameters has become possible.

We have, therefore, completed an initial long-term study of the calibration and housekeeping parameters of the Cluster FGM data on all four spacecraft. This work demonstrates the overall stability of the parameters from February 2001 to 2012, and is published in Geoscientific Instrumentation, Methods and Data Systems.[1] It has been discussed in detail in Section 4.5.

We have also dedicated some of our resource to cross-calibration efforts. A large number of data intervals (> 100) in C3 and C1 have been surveyed from 2001 to 2011 to compare the total B field measurements of FGM and EDI. We observed no consistency in the percentage difference between B_{FGM} and B_{EDI}. In general, good agreement was found between both instruments (>99 %). There is no trend in the remaining difference between EDI and FGM. The results are discussed further in Section 5.1.

Issues relating to FGM dataset definition and usability etc. are not discussed in detail in this document; these are presented in the accompanying User Guide [2].

2. Instrument Description

Each Cluster spacecraft carries an identical FGM instrument (Fluxgate Magnetometer) magnetic field to measure the DC magnetic field in the range DC to 10 Hz [3,4]. Each instrument, in turn, consists of two triaxial fluxgate magnetometers and an onboard data processing unit. The magnetometers are similar to many previous instruments flown in Earth-orbit and on other, planetary and interplanetary missions. In order to minimise the magnetic background of the spacecraft, one of the magnetometer sensors (the outboard, or OB sensor) is located at the end of one of the two 5.2 m radial booms of the spacecraft, the other (the inboard, or IB sensor) at 1.5 m inboard from the end of the boom. In flight, either sensor can be designated as the Primary Sensor, for acquiring the main data stream of the magnetic field vectors. In the default configuration, the OB sensor is used as the Primary Sensor. The instrument is designed to be highly failure-tolerant through a full redundancy of all its functions. The magnetometers can measure the three components of the field in six ranges with full scales and corresponding digital resolutions as shown in Table 1. From November 2000 to October 2006, ranges 2–4 (see Table 1) were in regular use. Starting in

November 2006, range 5 entered routine use. Starting in May 2008, range 6 entered routine use. Starting in December 2009, range 7 entered routine use. Neither range 6 nor range 7 was originally intended for use during the nominal mission hence these ranges were not fully calibrated on the ground.

RANGE NUMBER	RANGE	RESOLUTION
2	- 64 nT to + 63.97 nT	7.8×10^{-3} nT
3	- 256 nT to + 255.87 nT	3.1×10^{-3} nT
4	- 1,024 nT to + 1,023.5 nT	0.125 nT
5	- 4,096 nT to + 4,094 nT	0.5 nT
6	- 16,385 to + 16,376 nT	2 nT
7	-65,536 to + 65,536 nT	8 nT

Table 1: FGM Operating Ranges and Resolution

Switching between ranges is either automatic, controlled by the instrument Data Processing Unit (DPU) in flight, or set by ground command. When in the automatic mode, a range selection algorithm running in the DPU continuously monitors each component of the measured field vector. If any component exceeds a fraction (set at 90%) of the range, an up-range command is generated and transmitted to the sensor at the start of a new telemetry format. (All three components are measured in the same range.) If all three components are smaller than 12.5% of the range for more than a complete spin period (implemented as more than a telemetry reset period, or 5.15222 s), a downrange command is implemented at the start of the next telemetry format.

The sampling of vectors from the magnetometer sensor designated as the primary sensor is carried out at a rate of 201.75 vectors/second. This internal sampling rate has been selected to provide an appropriate set of lower rates (after filtering) for the different telemetry modes. In order to ensure the high stability of the sampling rate, the clock signal used for it is derived from a 2^{23} Hz crystal oscillator internal to the instrument. The primary requirement is that the sampling of vectors be carried out at equal time intervals. This requirement is implemented by sequencing the software by the sampling clock and by ensuring that all software sequences have a deterministic duration.

The full bandwidth of the sampled vectors cannot be routinely transmitted via the telemetry because of the limited telemetry rate allocation. The Central Processor Unit convolves the full bandwidth data with a Gaussian digital filter to match the rate and bandwidth of the transmitted vectors to the available telemetry rate. The filter coefficients are selected from stored sets corresponding to the different telemetry modes.

FGM full-resolution data consist of time series of magnetic field vectors for each of the four spacecraft, with the time resolution defined by the spacecraft telemetry mode and the FGM telemetry. The most frequently used FGM telemetry modes are indicated in bold in Table 2. Notice that the FGM calibration is based on the outboard sensor measurement and the inboard sensor data are not routinely used.

Spacecraft TM modes	FGM telemetry modes	Vector/s (primary sensor)	Vectors/s (secondary sensor)
Nominal Modes 1, 2, 3 and Burst Mode 2	A	15.519	1.091
	B	18.341	6.957
	C	**22.416**	**3.011**
Burst Mode 1	**D**	**67.249**	**7.759**
Burst Mode 3	F	F (MSA dump)	

Table 2: FGM vector rates where MSA stands for Micro Structure Analyser (the FGM Internal Burst Memory Device)

The fluxgate sensors are most sensitive in the range 0 Hz to 10 Hz. The signal chain from the sensor acquisition to the telemetered data stream has two filter stages – an anti-aliasing analogue filter on the output of the raw sensor voltage and the DPU implemented digital filter(s) described above (See Figures 5 and 6 in [3]). The FGM is a DC Magnetometer - while the sample rate in Burst Mode is 67 vectors per second the target application of this mode is high resolution time sampling of discontinuity structures such the bow shock or magnetopause. Caution is therefore required when interpreting FGM data in the frequency domain as the wave power will not be accurate above 10Hz due to the filter cut-offs and it is likely the STAFF search coil dataset will be more accurate. The overall instrument frequency response up to 100Hz along 3 axes of the FEE (Front End Electronics) from spacecraft 3 measured during ground calibration is shown in Figure 1. The -3dB point for Normal mode is 8Hz and 17Hz for Burst mode.

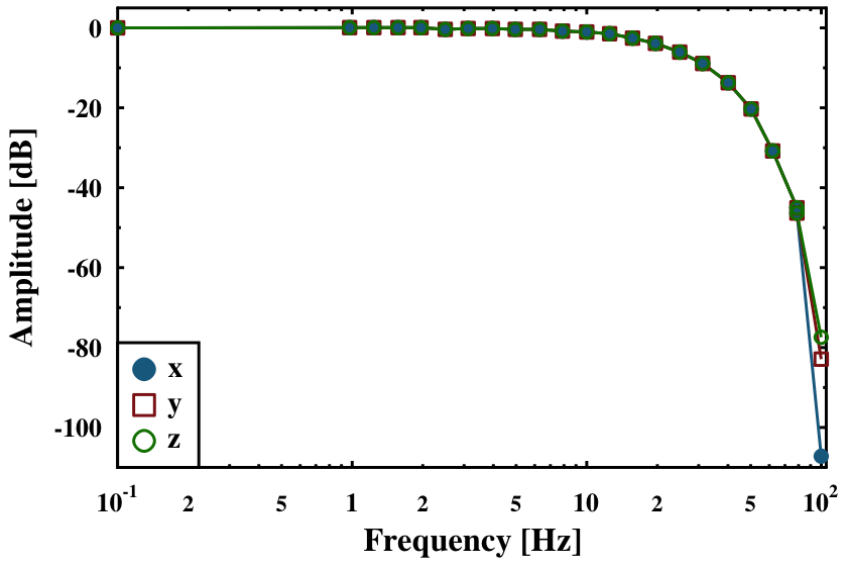

Figure 1:The overall instrument frequency response of the FEE unit from spacecraft 3 along 3 axes to 100Hz.

The in-flight calibration of FGM is based on an evaluation of all the possible sources of errors that occur in the measurement process, embodied in an "instrument model" representing the measurement processes of the magnetic field. Conceptually, the actual value of the ambient magnetic field vector at the location of the FGM sensor (given, for instance, in Geocentric Solar-Ecliptic, GSE, coordinates, as BGSE) is measured by the FGM output through the telemetry as a digitised vector V. This vector (the actual measurement) depends in a complex, but linear way on the alignment and orthogonality of the sensor axes with respect to the GSE coordinate system; on the scale factors and offsets of the sensors and electronics of FGM; and on the offsets introduced by the spacecraft. The instrument model also needs to take into account the time and frequency response in the form of delays and effective bandwidth due to the magnetometers, the Analogue-to-Digital Converters, and the digital filtering process. The coordinate transformation from GSE into the (nearly, but not quite orthogonal, see Figure 2 below) magnetometer sensor system (specific to each of the eight magnetometers on the four Cluster spacecraft) is a superposition of transformations that take into account also the misalignments introduced by the spacecraft, the magnetometer booms, sensor mounting and construction. All of which are required to be evaluated for each measured output vector.

3. Measurement Calibration Procedures

Figure 2: The relationship between the orthogonal (x,y,z) and sensor (S_1,S_2,S_3) coordinate systems. The angles θ and φ for each sensor coordinate are defined in the same way. The task of producing calibrated data then comes down to determining the parameters in this calibration equation. There are six angles, three gains and three offsets. There is no single calibration analysis that can be used to calculate all of these parameters. S3 has been omitted for clarity. See [1] for more detail.

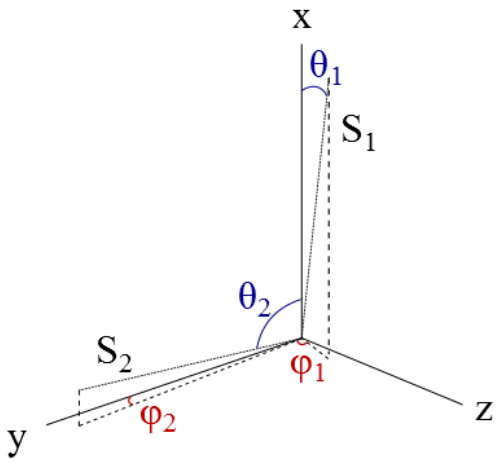

The calibration of the magnetic field data is of key importance for meeting the scientific objectives not only of the magnetic field investigation, but also those of the mission as a whole, as the interpretation of observations in terms of physical processes relies on the detailed comparison of measurements made at the four spacecraft.

Calibration in this context represents the determination of parameters that allow the transformation of raw measurements transmitted through the telemetry into a magnetic field vector, given in physical units (nT), in an instrument-specific coordinate system that is unambiguously related to the coordinate system of the spacecraft. The calibration parameters are used by the FGM data processing software to generate the magnetometer data in a range of geophysical coordinate systems.

Ground calibration of the FGM instruments has allowed the development of a practical model of the instruments, identifying the effective transformations that lead from the ambient field to the measured output in the following form:

$$\mathrm{V} = \underline{\underline{c}}^{(instr)}\,\underline{\underline{c}}^{(SR-FSR)}\,\underline{\underline{c}}^{(spin)}\,\underline{\underline{c}}^{(att)}\,\mathrm{B}_{GSE} + \mathrm{c}_0$$

where SR and FSR refer to (Spacecraft) Spin Reference and FGM Spin Reference frames and (SR-FSR) denotes the transformation matrix between the two. The sensor matrix $\underline{\underline{c}}^{(sensor)} = \underline{\underline{c}}^{(instr)}\,\underline{\underline{c}}^{(SR-FSR)}$ represents the sensitivities (scale factors) of the sensors and the alignment of the three sensor axes with respect to an orthogonal coordinate system aligned with the real spin axis. The spacecraft spin is taken into account in the rotation matrix $\underline{\underline{c}}^{(spin)}$, corresponding to the spin-phase angle of sensors at the time of the measurement. The matrix $\underline{\underline{c}}^{(att)}$ represents the transformation into the spacecraft spin-aligned coordinate system from the GSE system. This matrix is determined from the spacecraft attitude measurements. Finally, the vector $\mathbf{c}_0$ represents the offsets associated with the sensors and the spacecraft background field at the location of the sensors.

The equation defining the measurements can be transformed to state the in-flight calibration task, which is to determine the relevant term in the inverted form of this equation:

$$\mathrm{B}_{GSE} = \underline{\underline{c}}^{(att)^{-1}} \underline{\underline{c}}^{(spin)^{-1}} \underline{\underline{c}}^{(SR-FSR)^{-1}} \underline{\underline{c}}^{(instr)^{-1}} \left(\mathrm{V} - \mathrm{c}_0\right)$$

In the following, the steps performed by the first modules of the data processing software are described that implement the practical definition of the calibration parameters that need to be derived from the data. The digital output of the magnetometer is a vector **V** in binary units. As a preparatory step, this vector is transformed into physical units, using a diagonal matrix of nominal scale factors, $\underline{\underline{\mathrm{M}}}_{ST}$ (nT/binary count), to a vector, $\mathbf{B}_{FS}$ corresponding to the tri-axial magnetometer output in magnetic field units (uncalibrated, or "raw" nT):

$$\mathbf{B}_{FS} = \underline{\underline{\mathrm{M}}}_{ST}\, \mathbf{V}$$

where FS refers to FGM Spinning and ST to Scale factor Transformation. The coordinate system used in this equation is the FGM sensor system, defined by the true (magnetic) directions of the sensor triad; it is not exactly orthogonal, due to small inaccuracies in the magnetic and mechanical alignment of the sensors. The vector $\mathbf{B}_{FS}$ is used as an input to the next processing step which uses the calibration parameters to yield the magnetic field vector in physical units, in a coordinate system, denoted *FSR*, which is the FGM spin reference system, an orthogonal, right handed coordinate system with its x-axis along the real spin axis of the spacecraft, and the y-axis aligned with the sensor along the magnetometer boom. The defining equation of this transformation is,

$$\mathbf{B}_{FSR} = \underline{\underline{\mathrm{c}}}^{cal}\, \mathbf{B}_{FS} - \mathbf{o}^{cal}$$

.

The objective of the in-flight calibration therefore is to determine the 3 x 3 matrix, $\underline{\underline{\mathrm{c}}}^{cal}$ and the offset vector, $\mathbf{o}^{cal}$, used in this equation for all magnetometers on the four spacecraft, for all ranges and, in each case, for both A-D converters. The calibration matrix, $\underline{\underline{\mathrm{c}}}^{cal}$ depends on a number of effects that include range-dependent scale factors, deviations of the sensor axes from orthogonality, scale factor deviations between the two A-D converters and alignment of the sensor axes to the spin axis system. The offset vector, $\mathbf{o}^{cal}$, depends on both spacecraft-induced and sensor offsets. Despinning, i.e. the application of the matrix, $\underline{\underline{c}}^{(spin)^{-1}}$, as well as the coordinate transformation, $\underline{\underline{c}}^{(att)^{-1}}$ into a physical coordinate system, such as *GSE*, is performed in the routine data processing of the FGM data and are not discussed further here.

In summary, to fully define the transformation for the three sensors, 9 matrix elements and 3 offsets are required for each of the ranges used. Some of these parameters are defined using measurements made before launch. In the approach that we use it is not possible to determine the remaining calibration parameters through the application of a single method. Suites of methods are available, described briefly below, and each calibration file is derived using a combination of these. Each calibration file contains details of the elements of the calibration pipeline that were used in its derivation (shown in Figure 3, below). The time interval to which each method is applied varies for each technique, as described below.

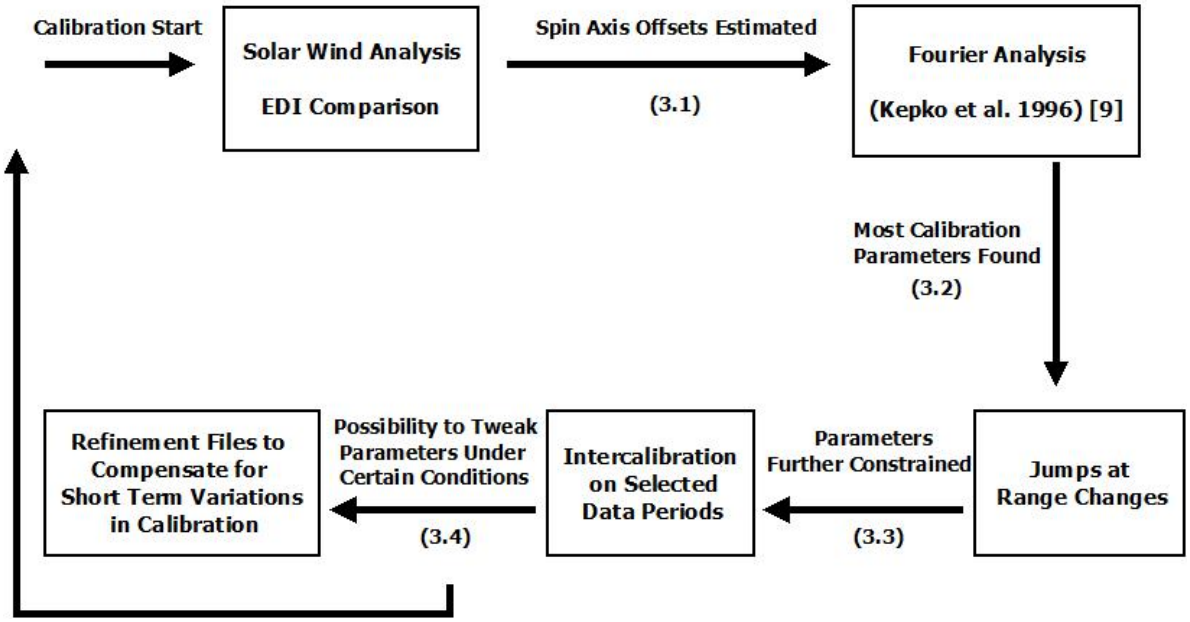

Figure 3: The calibration procedure for the Cluster Active Archive with numbers relating to the steps in the text below.

The selection of methods employed in the derivation of each calibration file depends on the properties of the data and affects the accuracy of the final calibration. All methods lead to the derivation of a calibration file valid for a single orbit, defined perigee to perigee, with the exception of the last method discussed below, which allows us to estimate the variation of the calibration parameters within a single orbit, introduced by eclipses for example. These short-term variations would act as a refinement to the orbit calibration files. However, in the interest of maintaining the data delivery schedule, we have given higher priority to generating the orbit calibration files, and the procedure for routine derivation of calibration refinement files is still in development.

A number of methods are employed to determine calibration orbit files. Specifically these are listed as:

- *Estimation of offset on spin-aligned sensor*
- *Application of Kepko calibration analysis*
- *Refinement of calibration parameters based on jumps in B at range changes*
- *Inter-spacecraft calibration*:

3.1. Estimation of offset on spin-aligned sensor

Three methods exist by which the offset on the sensor aligned with spacecraft spin axis can be estimated:

3.1.1. Estimation of the FGM spin axis offset using solar wind observations.

(This section is taken from Alconcel et al. section 2.3 [1].) In general, the four Cluster spacecraft sample the solar wind from mid-December to mid-April, a period which is known as the “dayside” season. During this period, the magnetic field in the solar wind is used to adjust the offset (O_1) associated with the axis of the sensor that is aligned with the spin axis of the spacecraft. FGM is nearly always in range 2 during these periods, so this is the only range for which this method can be used to refine the spin-axis offset. This procedure is based on the observation that fluctuations in the solar wind magnetic

field are primarily rotational, which means that there should be no correlation between the spin-axis component of the magnetic field and the total field magnitude[5].

The procedure works by searching through the spin-averaged data for rotational discontinuities. At these discontinuities, O_1 is adjusted to minimise the correlation between B_1 and |B|. In general, 1 month's worth of data is divided in half and adjustments are applied separately to the first and second halves of the month. The implementation of this procedure was originally developed by FGM co-investigators at UCLA (University of California Los Angeles; personal communication with H. K. Schwarzl, K. Khurana, and M. Kivelson, 2005) who have collaborated with the FGM team on its implementation at Imperial College. A complete description of the theory underlying this method can be found in Hedgecock (1975) [5].

From mid-April to mid-December the four Cluster spacecraft sample Earth's magnetotail, a period which is known as the "nightside" or "tail" season. The technique described above cannot be applied to this data to adjust the spin-axis offset. A simple linear interpolation of the offset between the last solar wind measurement in mid-April and the first solar wind measurement in mid-December is performed instead. This method likely masks the natural variation in the offset during these periods.

3.1.2. Refinement of the estimation of the spin axis offset based on solar wind observations.

For intervals of exceptionally quiet solar wind data it is sometimes possible to further refine the parameters. However it is unusual to find periods that are quiet enough to distinguish the small and stable differences between the spacecraft which are necessary in order to refine the parameters. Therefore this procedure is used only rarely. The solar wind refinement method has been used on the February 2003, the second half of January 2004 and the first half of March 2004 data.

3.1.3. Use of EDI time of flight measurements in monitoring FGM spin axis offset.

When Cluster is located in the magnetospheric tail and no solar wind data are available, it is possible to monitor the offset on the sensor aligned with the spin axis using the absolute |B| measurements available from the Electron Drift Instrument (EDI). EDI measures the displacement of a beam of test electrons after they have completed one gyration around the local magnetic field. The electron time of flight information is therefore related to the value of |B|. Comparisons can be made between FGM and EDI. The time of flight measurements are converted into absolute |B| data and the statistics gained through the comparison of these measurements with the FGM data should in principle make it possible to estimate corrections to the spin axis offsets of the FGM sensors.

A minimisation technique developed by the FGM team has shown using simulated data that it is in principle possible to extract spin axis offset corrections up to a particular level of noise on the EDI data in ranges 2-4. The instantaneous EDI values have a quite high noise level (~2-3% or even more), but the average values remain stable which can be used for comparison. Additional difficulty arises from the length of the code repetition frequency of EDI: it turns out that the value of the electron gyroperiod measured by EDI depends on this parameter. A change of code repetition frequency shows a step-like change in the electron gyroperiod. It would also be a requirement for the inter-spacecraft distance to be a maximum of 4000 km for datasets to be cross-calibrated and the periods for which this holds would be minimal. Additionally, these comparisons could mostly be applied to spacecraft 1 and 3 as EDI was never operational on spacecraft 4 and stopped active operations on spacecraft 2 in April 2004. Comparisons could be carried out throughout the year.

The offset corrections used in the CAA datasets during the tail seasons (approximately from June until November) are currently based on the interpolation of the offsets between two consequent dayside seasons (approximately from November to May).[1] Figures 4-6 show 55 minutes of spacecraft 3 data from September 2010. This data is from the tail season where

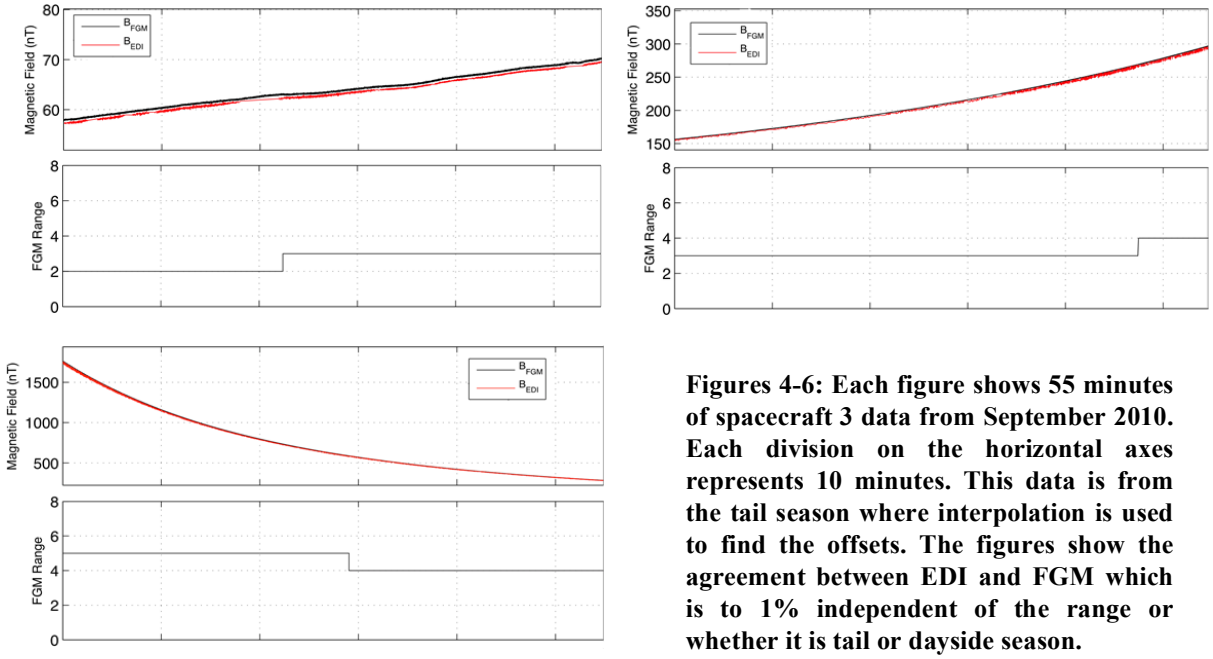

Figures 4-6: Each figure shows 55 minutes of spacecraft 3 data from September 2010. Each division on the horizontal axes represents 10 minutes. This data is from the tail season where interpolation is used to find the offsets. The figures show the agreement between EDI and FGM which is to 1% independent of the range or whether it is tail or dayside season.

interpolation is used to find the offsets. The figures show EDI and FGM agree to within 1%. This is independent of the range or whether it is tail or dayside season

Although such comparisons could potentially be used to adjust the spin axis offsets during the Tail Season when the solar wind method cannot be applied, the FGM team has opted not to do this. The method could only be applied on two spacecraft, which would lead to a lack of consistency between the FGM datasets. Additionally, the long-term trends study [1] and the survey of EDI/FGM comparisons shown in section 5.1 have shown that the interpolation method is consistently adequate. The agreement between EDI and FGM is greater than 99% over ten years and multiple instrument ranges/modes in nearly every instance analysed.

3.2. Application of Fourier (Kepko) calibration analysis

The calibration method described by Kepko et al. [9] uses an iterative technique to determine eight of the twelve calibration parameters, although two of these are relative rather than absolute values. This method is applied to every orbit and is used in the calculation of every calibration file. The Fourier analysis technique employed by Kepko is the central calibration method. The method is based on the fact that these eight calibration parameters, when incorrect, produce spin harmonic signatures in the magnetic field data. These spin harmonics can be measured and related to the corrections to the calibration parameters in question. The set of equations which relate the properties of the spin harmonics to the corrections to the calibration parameters are first linearised and then solved iteratively. A satisfactory solution is usually obtained within very few (6-8) iterations.

3.3. Refinement of calibration parameters based on jumps in B at range changes

This method uses the information that the magnetic field should be continuous across range changes of the instrument. Any change in **B** observed at a change of instrument range can be ascribed to inaccuracies in a subset of the calibration parameters and therefore under quiet field conditions, where the jumps in **B** are of larger amplitude than the natural variance of the magnetic field being measured, the size of the jumps can be used to further constrain and refine some calibration parameters.

Data from either two weeks or one month are required as input to this technique, since in order for the observed magnetic field jump across a range change to be included in the statistics, the variance of the measured magnetic field must be lower than the jump introduced by the errors in the calibration parameters. If the spacecraft are in an environment where the background magnetic field fluctuations are large, in the magnetosheath for example, data from a month are usually required. This data is applied as part of the routine calibration procedure to data from every orbit.

3.4. Inter-spacecraft calibration

A method of inter-calibrating four spacecraft was developed by Khurana [10], which uses the principle that in some parts of the magnetosphere the current density is zero, measured by estimating Curl **B**, together with the information that Div **B** is zero everywhere. This method can only be applied when the spacecraft are relatively close together, such that the estimates of Curl **B** and Div **B** from the four-spacecraft data are sufficiently accurate to constrain the calibration parameters. The method has been used by the FGM co-investigators at UCLA [10] and we have implemented the method at Imperial College for application to the 2003 tail season data where the spacecraft separation was suitably small (~250 km). Although the inter-spacecraft calibration analysis has also been performed on the 2001 tail season, significant improvements to the calibration quality were not found in this case.

4. Results of Calibration Activities

The full calibration process involves a calibration carried out on the ground before launch followed by constant in-flight calibration after the launch known as orbit calibration.

Though it is recognised that calibration is most difficult during eclipses, the relative accuracy between the four instruments of science data post-calibration is typically estimated to be in the range of 0.1 – 0.2 nT for magnetic fields less than 200 nT, i.e. |B| < 200 nT, and approximately 0.4 nT for magnetic fields greater than 200 nT and less than 4000 nT, i.e. 200nT < |B| < 4000nT, for Ranges 2, 3 and 4 with typical background power of the order of $2\times10\text{-}4\ nT^2/Hz$. The absolute accuracy is under continuous study with the agreements between FGM and EDI/WHISPER discussed in Section 5.1. Supporting caveat (CAVF) files are also routinely generated summarising the output of the orbit calibration pipeline.

4.1. Spin tone

Signatures of imperfect calibration might be seen in a number of ways within the data. The most generally visible signature is the occurrence of a pure signal at the spin frequency and/or at its harmonics within the data. The peak-to-peak amplitude of this signal depends not only on the size of the calibration parameter error, but also on the strength of the background magnetic field. At the highest values of |B| encountered at perigee, a peak-to-peak spin tone of up to 0.4 nT in Range 4 or 5 might be observed. Larger values occur in recent years when measurements have been made in Range 6 and Range 7. If the spin tone significantly exceeds these limits, a caveat is recorded. Spin tone thresholds for the caveat files are described in section 5.3 of the User Guide [2]. In lower fields, less than 200 nT for example, the spin tone tends to be of an

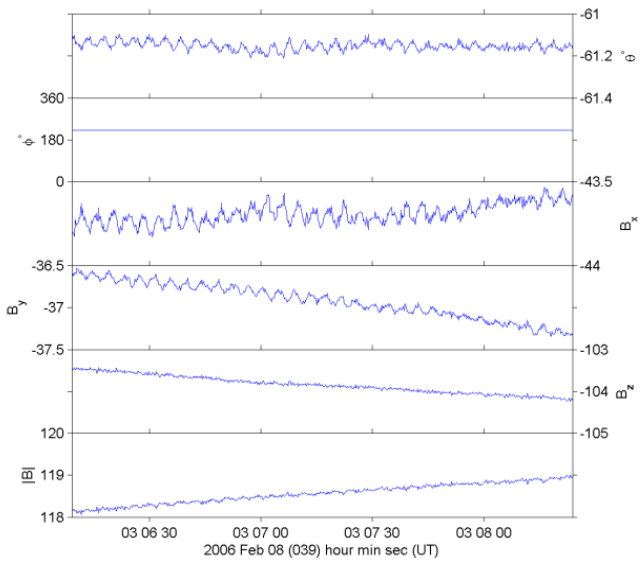

Figure 7: An example of small amplitude residual spin tone in Cluster 2 data from February 2006.

amplitude lower than 0.2 nT. An example of this signal is shown in Figure 7.

However, the FGM instrument on Cluster 1 is known to have a small spin ripple that is not a calibration effect, but is spacecraft generated, though the source is unknown. It has the similar characteristics to the data shown in Figure 7, but cannot be removed through calibration.

Since September 2010, bursty spin noise has been observed on C4. There appears to be no correlation to FGM or platform commanding. The periods are therefore caveated in Ranges 2 and 3, and are under continued investigation.

A particularly stark example of bursty spin noise from the September 2010 data is shown in Figure 8.

Figure 8: Bursty spin noise on C4 in Orbit 1574, shown in magenta. (C1 is black, C2 is red and C4 is green.) The sudden dramatic jump in spin noise lasts for about ten minutes, although intervals as short as five seconds and as long as half an hour have also been observed.

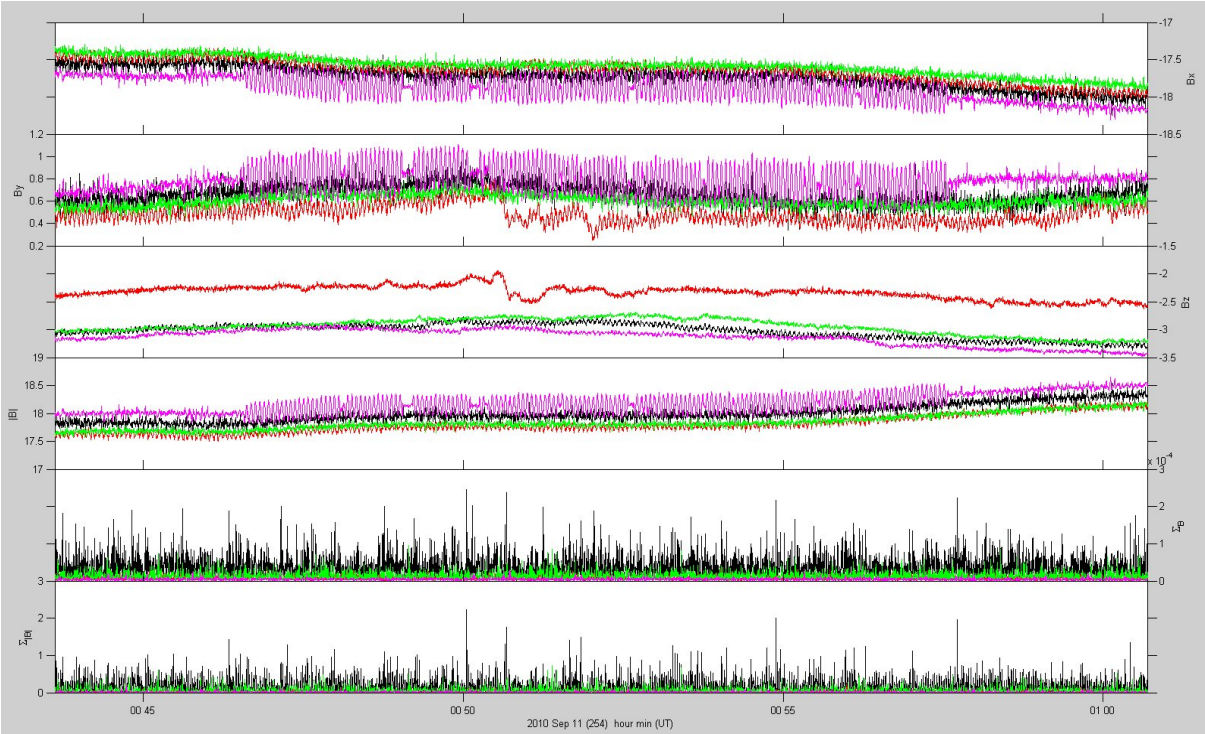

4.2. Range jumps

A second signature of an inaccuracy in the calibration matrix can sometimes be seen as a small jump in the magnetic field when the FGM instrument changes range. We expect the natural signal to be continuous across a range change, and so we interpret any magnetic field jump as a signature of a residual error in the calibration parameters. Minimising these jumps is done as part of the routine calibration procedure. The minimisation procedure involves adjustment of calibration parameters in both upper and lower ranges, as described in [1]. Figure 9 shows a case where the jump is almost completely eliminated as a result of the calibration. However, on some occasions the jump cannot be entirely removed, and a signature similar to the top three panels of Figure 9 might be seen in the final data, although the absolute size of the jump is generally much smaller. Typical residual changes in magnetic field magnitude are smaller than 0.2 nT in low fields (Range 2), and up to 0.5 nT in Ranges 3 and 4. The determination of the offsets and gains for Ranges 6 and 7 are dependent on the Range 5 calibrated data. However, changes in direction are generally less than a degree, and often < 0.1 degree.

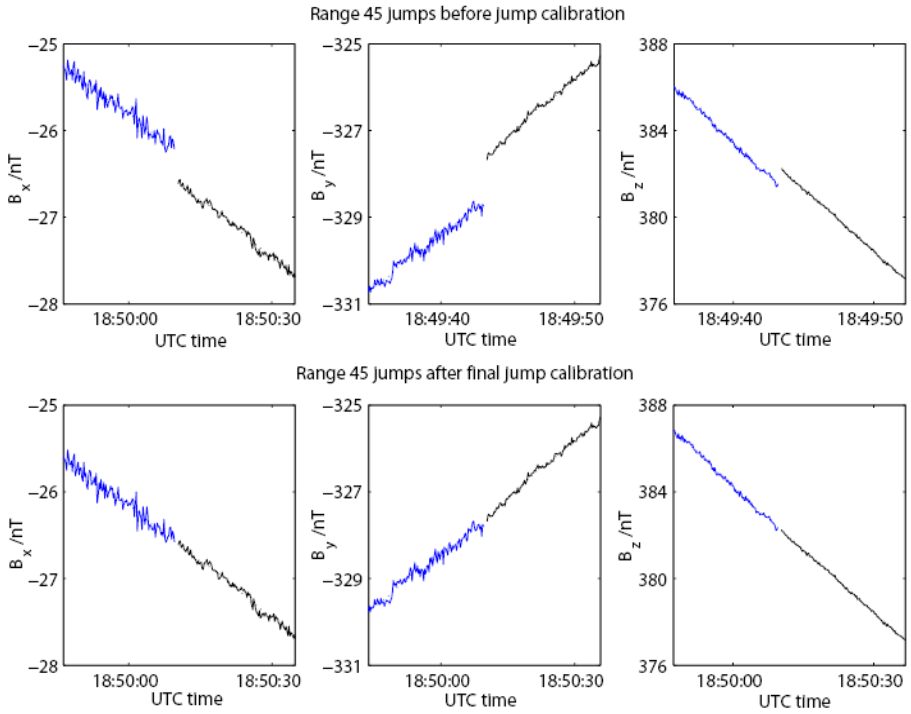

Figure 9: A typical figure generated during the range change analysis. The data are from 30th of January 2009. The upper three plots correspond to a Range 4-5 jump for each field component utilising the calibration file produced by the Fourier analysis step. The lower panel shows the same jumps after the corrected file has been further modified by the range change analysis. We can see on all three components that the jump offset has been reduced to almost zero and the data are now continuous across the range change.

4.3. Visual inspection of calibration quality

Spectrograms of single FGM orbital periods are also routinely used - as an indicator of the magnetometer calibration error. An example of a typical before and after calibration can be seen in Figure 10, which displays residual spin (0.25Hz and 0.5Hz) harmonics (tone) within the data. In order to check that the derived calibration parameters have the desired effect of removing the residual spin harmonics from the data, spectrograms are generated of the finalized data. These are visually compared with original spectrograms that are generated using the initial calibration files to establish if improvement has been made and to check any additional error has not been introduced. The left hand picture in Figure10 has been generated using initial calibration parameters for each range. The right hand picture shows the result of a refinement of the calibration based on visual inspection. Each range has its calibration refined separately.

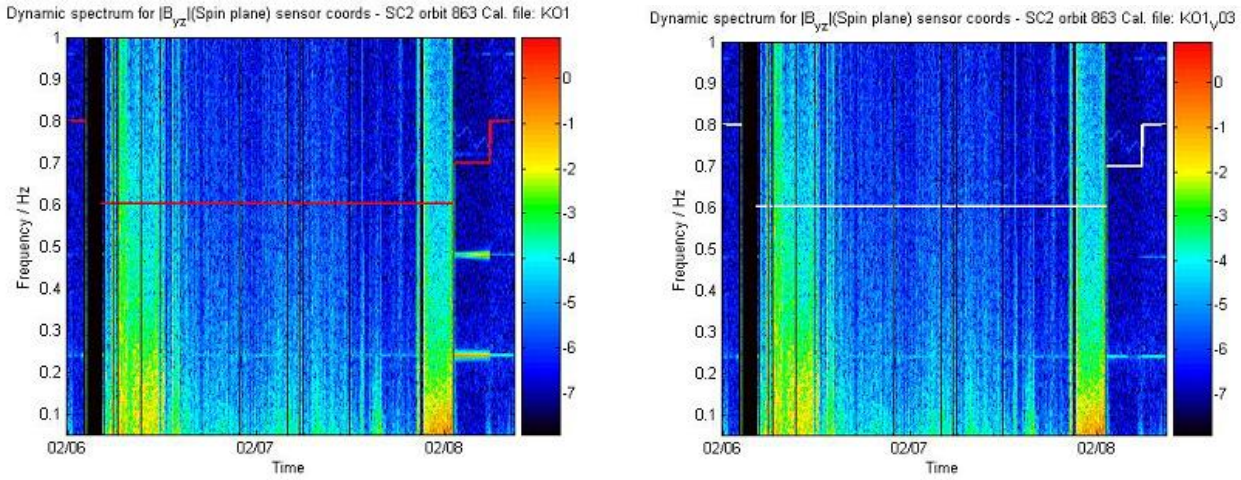

Figure 10: Showing spectrograms for orbit 863 (taken from February 2006) of the spin plane magnetic field magnitude before (left) and after (right) orbit calibration has been applied. The stepped red line in the left hand panel and stepped white line in the right hand panel indicate the instrument range for context, where the lowest line is Range 2. The two intervals of enhanced broadband power in Range 2 correspond to the magnetosheath.

As seen in Figure 10, the fundamental of the spin frequency is ~0.25 Hz (1 revolution of the spacecraft approximately every 4 seconds). It is present with unacceptable levels of spin-frequency signal and harmonics in the initial spectrogram in Range 3, at the start of 02/08. Full orbit calibration results in reduced harmonics across the range as indicated in the right side image. Although a significant improvement was achieved by orbit calibration, the 0.5 Hz spin-frequency signal (the second harmonic) across Ranges 3 and 4 indicates that the data was not well calibrated in the first instance.

4.4. Effects of High Powered Amplifier on Cluster 1

A signature on Cluster 1 of HPA (High Powered Amplifier) mode switching between High Power, Low Power and Off is observed as an offset in the spin-axis field (which is approximately equal to the z-Axis for the Spin Reference and Geocentric Solar Ecliptic reference frames). Figure 11 shows the allowed mode transitions for the HPA. Only Cluster 1 is affected due to the use on that spacecraft of a Travelling Wave Tube power amplifier. Datasets prior to February 2010 have these offsets steps included in the data which are flagged in the associated caveat file. Transitions prior to late 2009 were so rare that a caveat approach was deemed reasonable. However since this period HPA mode switching has become much more regular and this has necessitated offset removal in the time series using a pre-processing step. Data from Dec 2009 onwards have the HPA induced offsets corrected within the data processing pipeline.

The HPA induced offsets are stable and so a fixed value is subtracted from the data depending on what is the mode status of the HPA. The offset when the HPA was in Low mode is 0.66 nT and when the HPA is Off mode, 1.0 nT, see Table 3. These are now routinely applied during the pre-processing of the data prior to the solar wind analysis.

Mode Change	Mean Field Change [nT]	Standard Deviation [nT]
Off → Low	0.31	0.05
Low ↔ High	(-)0.66	0.1
High → Off	-1.0	0.1

Table 3:z-Axis field changes associated with each HPA mode change measured at the outboard sensor

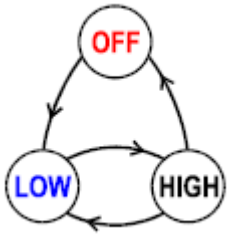

Figure 11: Mode transition diagram showing valid mode changes.

Figure 12 shows HPA activity affecting the Cluster 1 FGM data from October 2002. The bottom panel shows the offsets that occur when the mode is switched. The top panel shows the data set after corrections have been applied. The residual uncorrected vectors are then removed during the validation stage of the data processing. The uncorrected vectors are a result of the fact that the time of the switches cannot be extracted exactly; there is a resolution of 5 seconds. The times of all HPA mode switches are collated and these times specifically inspected for uncorrected vectors.

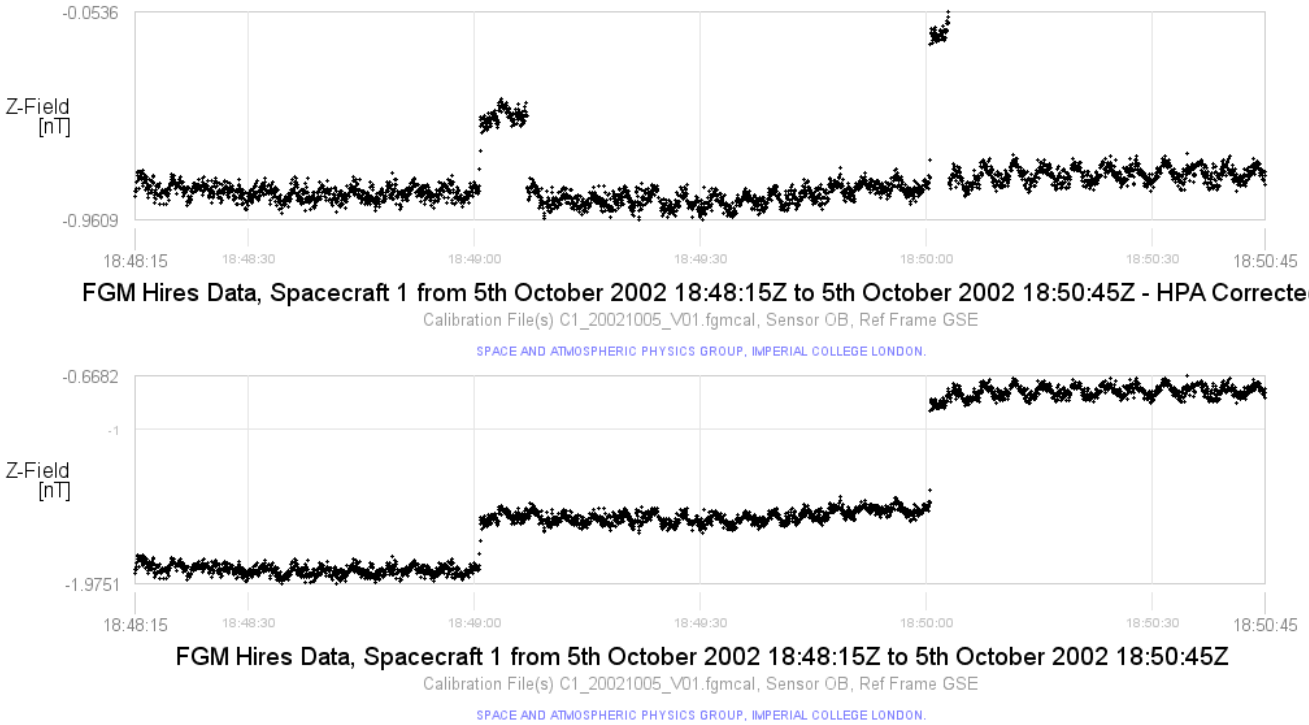

Figure 12: The offsets in the spin axis field that occur when the HPA mode switches between High Power, Low Power and Off, lower panel. These offsets are now corrected for in the calibration pipeline, top panel.

4.5. Long-term evolution of the calibration parameters

Routine calibration has now been carried out for all four spacecraft for data covering 13 years. Given that each instrument requires a separate calibration for each range, and that the calibration matrix for each range contains 12 elements, we have long-term statistics available for over 200 calibration parameters. Recently, we performed an initial survey of the

housekeeping and calibration parameters for the outboard sensors on all four spacecraft from February 2001 to February 2012. This work was submitted and has been published in GI [1].

Since we do not wish to belabour the analysis here, we will show a small selection of the data surveyed, with excerpts adapted from the text of the article. Figure 13 shows the outboard sensor temperature housekeeping parameter for all four spacecraft. Although each of these values is monitored more frequently, a single averaged value has been shown for each orbit (51-57 hours). The outboard sensor temperatures for all four spacecraft show a cyclical fluctuation over the course of nightside-to-dayside transitions, becoming around 5ºC warmer during the peak of the dayside season. The spikes are due to long eclipse periods, during which the FGM is off. All sensors have undergone a warming trend over the course of the mission as shown in Figure 13. Since the outboard FGM sensors are located on the ends of 5 metre booms, the warming and cooling cycle is most likely related to the spacecrafts' positions relative to the Sun during dayside and nightside seasons. The overall warming trend is likely related to the spacecrafts' positions relative to the Earth, as both periapsis and apoapsis have become lower over the course of the mission.

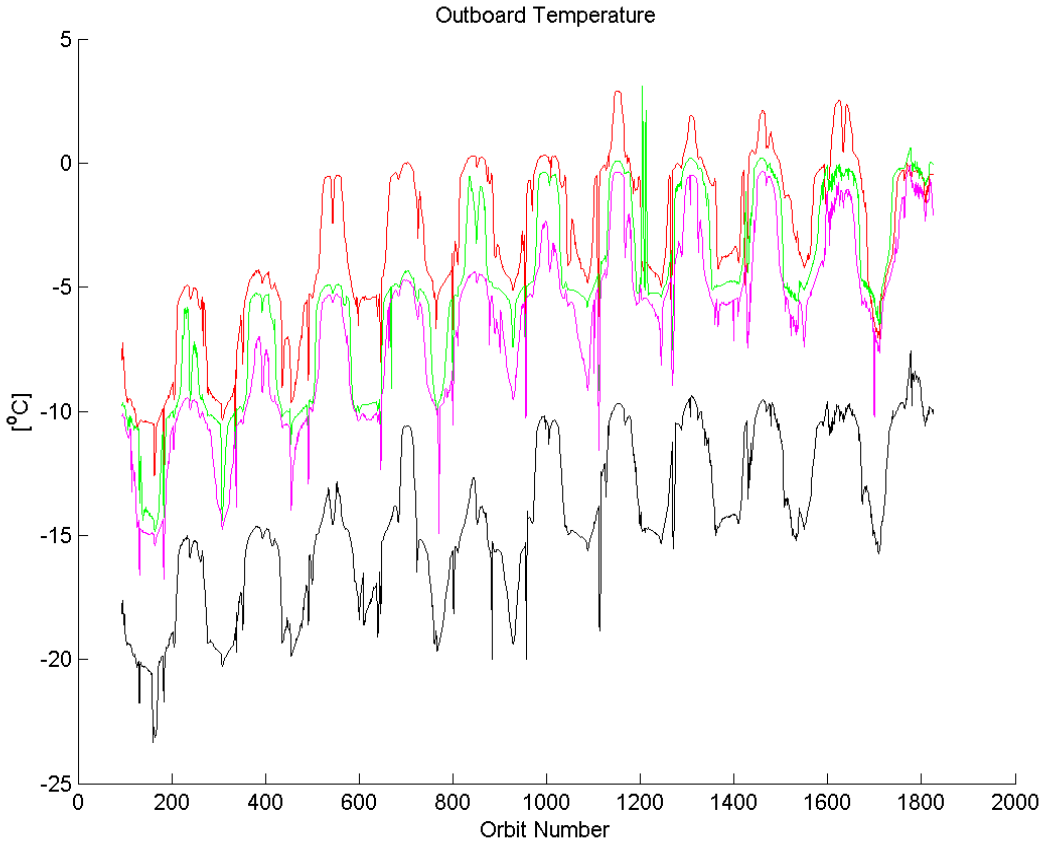

Figure 13. Outboard sensor temperatures in degrees Celsius for each spacecraft for Orbits 93 to 1889 (February 2001 through August 2012). C1=black, C2=red, C3=green, C4=magenta.

Figure 14 shows the spin-axis offsets for the four outboard sensors in the most sensitive range: Range 2, which covers the lowest magnetic field magnitudes (< 64 nT) The offsets vary little over the course of eleven years in C2, C3 and C4, although the C1 offsets appear to undergo a steady drift over the course of the mission. The biweekly/monthly adjustment of the spin-axis offset gives a short, step-like appearance to the offset lines, while the interpolation method gives longer sloping steps for the seven or so months (around 100 orbits) that the spacecraft spend on the nightside portion of their tours.

The interpolation appears to provide adequate estimates of the spin-axis offsets, though it is likely masking the natural parameter variability.

In the spin-plane offsets, which are computed on a per-orbit basis, a cyclical trend can be observed that seems to appear to track the electronics box and outboard sensor temperatures, rising and falling in the same cycle. In future, it might be desirable to perform a more thorough data correlation between calibration parameters and temperatures in order to try and discover a temperature coefficient which could be compared with ground data. This was deemed beyond the scope of the present work as an initial survey of parameter comparisons.

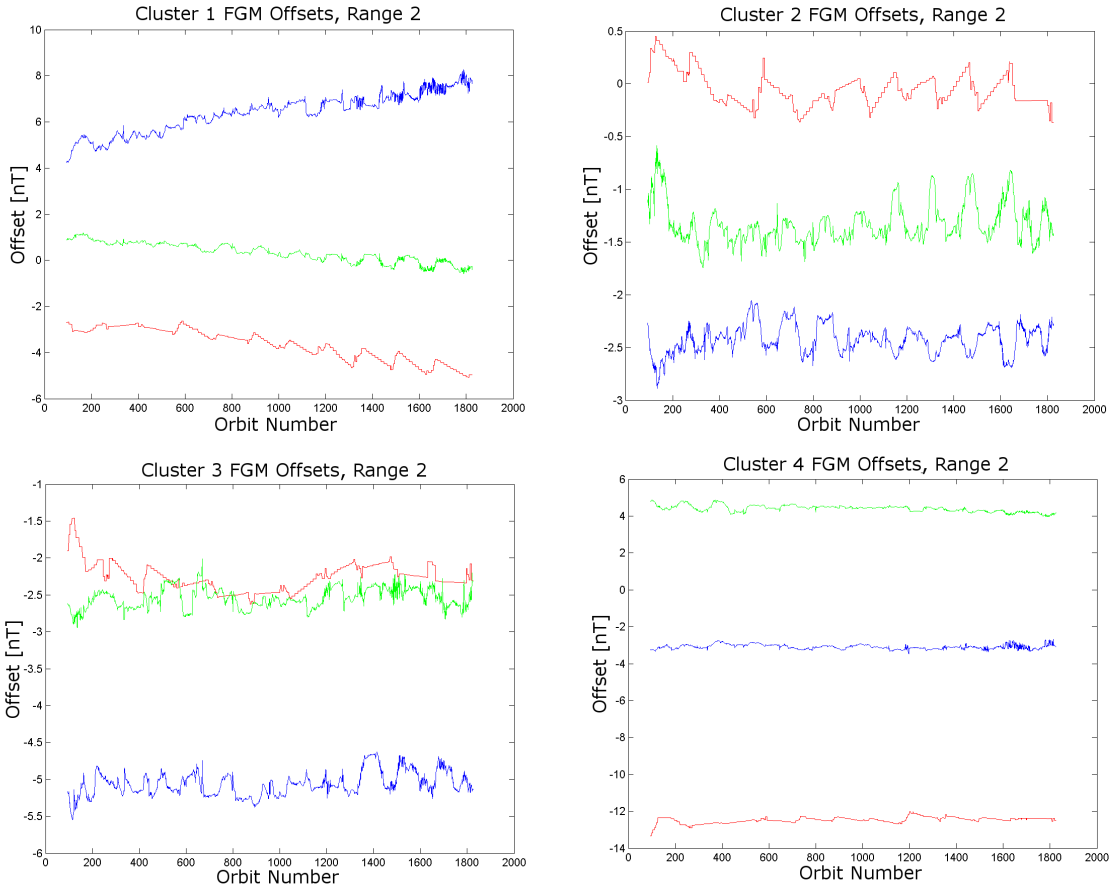

Figure 14. Offsets for all four spacecraft (C1-C4) from February 2001 to February 2012. Spin-axis offsets are shown in red while spin-plane offsets are in blue and green.

The other calibration parameters (gains, elevation angles and azimuthal angles) show similar consistency over the course of the mission. In Figure 15, the gains for all four spacecraft in Range 2 are shown. The spin-axis gain difference (ΔG_{32}) appears to undergo periodic increases in fluctuation, seemingly corresponding with the warming/cooling cycles observed in the instrument house-keeping sensor temperature values, as shown in Figure 13. However, both the gain difference and the azimuthal angle difference in the spin plane contribute to the second harmonic of the spin frequency used in the Fourier analysis. None of the calculated absolute angles exhibit this behaviour, which would suggest that the link to the temperature cycling may be coincidental. It is also possible that the phenomenon is noise-related. The data are much cleaner in the Tail season, which might lead to reduced fluctuation in the calculation of these parameters, for example. The potential causes cannot be distinguished easily and are beyond the scope of this initial investigation.

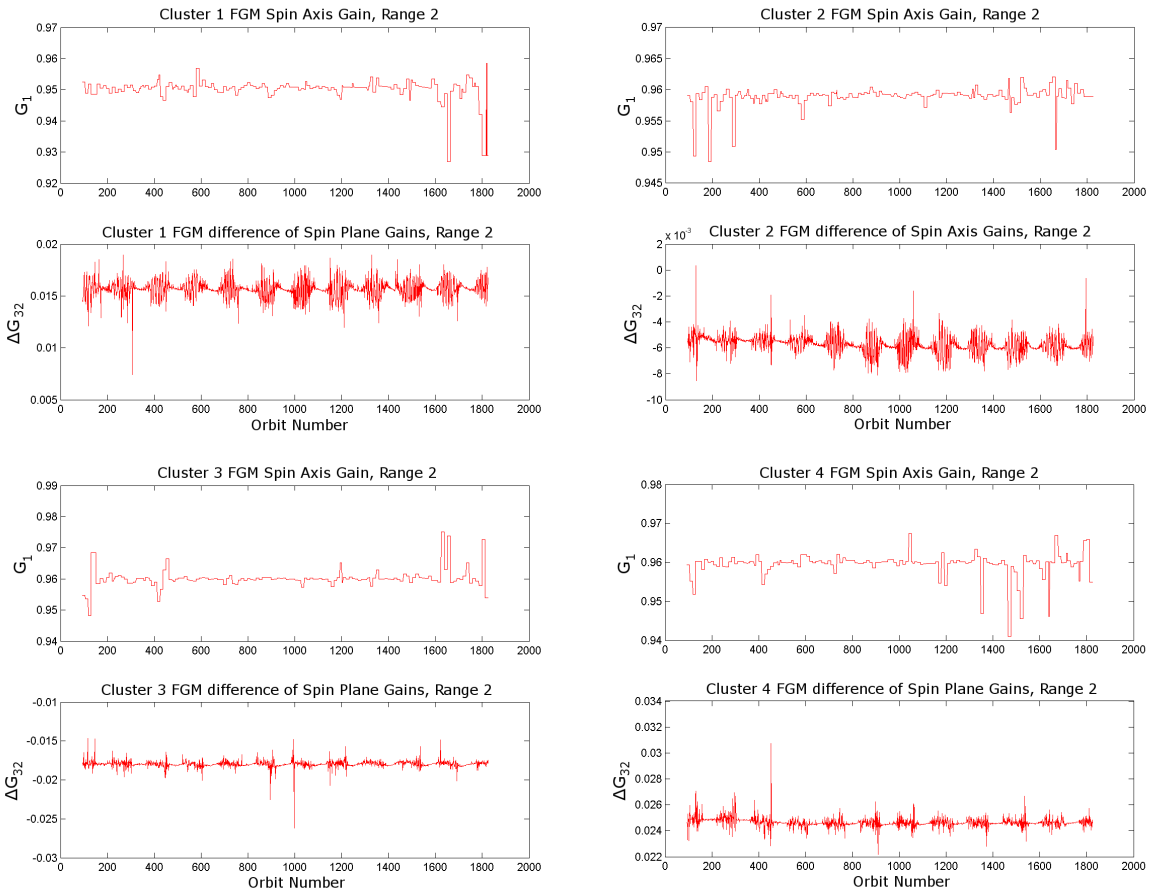

Figure 15. Gain plots (G_1 and ΔG_{32}) from Feburary 2001 to February 2012 showing periodic behaviour of spin-plane gain difference for Range 2 in all spacecraft.

Additionally, tabulated means and standard deviations were computed for all the parameters over the course of the mission. This, and a visual inspection of the plots, allowed us to easily identify orbits with egregiously problematic calibration. These periods of poor calibration were identified, corrected, and resubmitted to the CAA. Fortunately these periods were few (67 orbits out of ~1900). Redelivery took place between September and December 2013.

In general the stability of the outboard sensor calibration parameters over the course of the mission was demonstrated to be excellent. Hence, confidence can be placed in the accuracy of the Cluster magnetic field data.

5. Results of Cross-Calibration Activities

5.1. DC magnetic field

Cross calibration activities for the FGM DC magnetic field are limited to comparisons with the EDI and WHISPER which can produce a measure of the overall magnetic field magnitude. This magnitude figure can then be compared to the FGM magnitude on similar spacecraft. This permits estimation of the FGM spin axis offset that unlike the spin-plane components is not easily derived outside the solar wind due to the lack of regular 180-degree rotations.

As part of our cross-calibration efforts, a large number of data intervals (> 100) in C3 and C1 have been surveyed from 2001 to 2011 to compare the total B field measurements of FGM and EDI. The criteria applied to the data intervals were as follows:

- Small or no gaps in both FGM and EDI data
- Constant FGM range and EDI CRF mode
- 2-3 months between intervals
- C3 intervals selected first and C1 intervals used if the first two criteria were met

The percentage difference between FGM and EDI were calculated thusly: $(B_{EDI} - B_{FGM})/B_{EDI} * 100 = \Delta B_{EDI\text{-}FGM}$. The results for C3, plotted against the date and categorised according to FGM range, are shown below in Figure 16.

Figure 16: FGM-EDI comparison for C3.

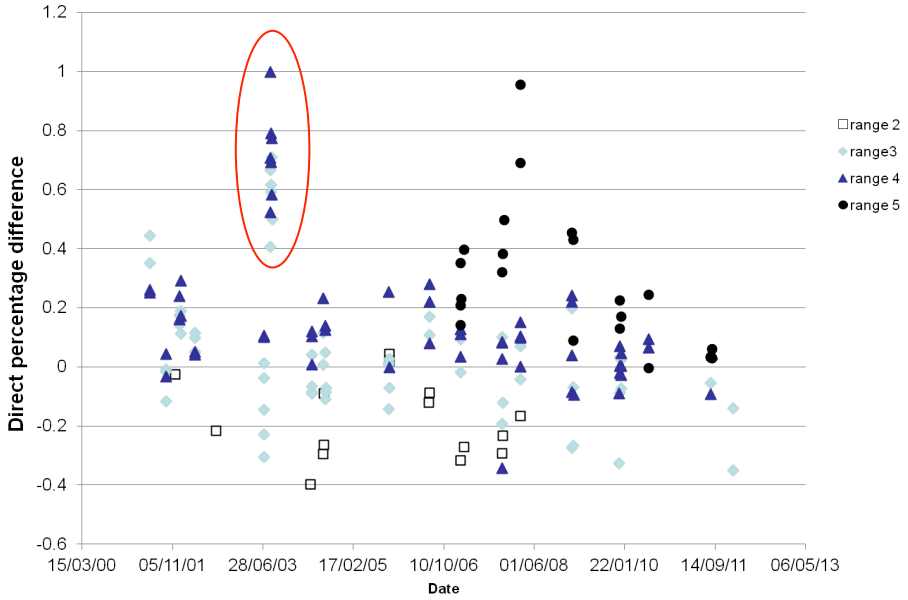

In general, good agreement between both instruments (>99%). It can be seen from this plot that $\Delta B_{EDI\text{-}FGM}$ ranges from -0.4% to 1.0% with no consistency. Additionally, $\Delta B_{EDI\text{-}FGM}$ seems to increase with FGM range. The case of August 2003 (circled in red) stands out, as it shows by far the largest $\Delta B_{EDI\text{-}FGM}$. This is true on both spacecraft as shown below in Figure 17. August 2003 is therefore not a good benchmark for treatment of differences between FGM and EDI.

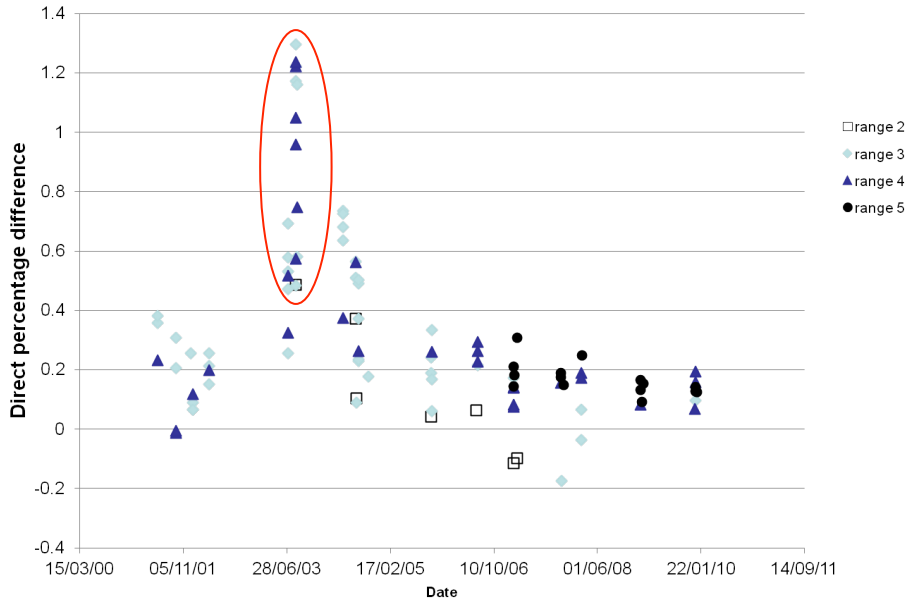

Figure 17: FGM-EDI comparison for C1.

In C1, apart from the anomalously large $\Delta B_{EDI-FGM}$ values for August 2003, the percentage difference shows no dependency on FGM range. This is also true for the EDI CRF mode (not shown here). The range of $\Delta B_{EDI-FGM}$ is slightly different from that observed in C3: -0.2% to 1.3%. Still, there is no consistent trend observed in the eleven years of data surveyed in the direct percentage difference between FGM and EDI.

The set of cross-calibration results indicates a discrepancy that is variable between -0.4% and 1.3% in EDI/FGM. It is 0.2% in WHISPER/FGM ratio comparisons. We plan to identify more intervals, intervals in higher FGM range and EDI CRF modes, attempt correlation with trajectory information and add a comparison with WHISPER data before 2006.

Efforts to understand the source of these discrepancies have been undertaken, including: the use of identical analysis periods for the EDI and WHISPER in order to achieve similar results, and filtering techniques to investigate if the results with larger errors associated with them were biasing the analysis. Despite these efforts, currently the source of the discrepancies has remained, with similar discrepancies found and presented by the EDI team when comparing EDI and WHISPER. This has cast uncertainty on which discrepancy may indicate a possible source of error, and although the source of the discrepancy is no closer to being found, it is the case that (the size of) the potential error within FGM data is a small concern.

It is also noted that even if part or all of the discrepancy is found to have its source in the FGM data there is no straightforward method to make the correction and it may turn out to be a highly complex problem. This is due to comparisons between EDI and WHISPER data may only be accomplished with magnetic field magnitudes, where the possible error within the FGM data would be spread between the gains on each of the three sensor components.

5.2. AC magnetic field

The fluxgate sensors are most sensitive in the range 0 Hz to 10 Hz as shown in Figure 1. In higher frequencies above 5 Hz it is often STAFF which is more sensitive and which provides more accurate wave amplitudes [11]. At frequencies above 1 Hz the fluxgate magnetometer tends to measure magnetic field amplitudes that are too low. CAA users wishing to study waves in the frequency range above ~5 Hz should note that FGM is a DC instrument, and that filters within the instrument will significantly attenuate wave power above this frequency. It is recommended that the search coil measurements from the STAFF instrument be used to analyse waves in this frequency range.

However, close to the spin frequency FGM despins the data better than STAFF. The STAFF and FGM spectra are continuous and very complimentary datasets. They can be merged as shown in [12]. It appears that the phase of the wave fluctuations is the same to within 2-3° between STAFF and FGM [11].

6. Summary

Routine calibration of FGM data and analysis of the calibration procedure are still ongoing. An absolute measure of the accuracy of the calibration is not possible but is under continuous study. However, the relative accuracy inferred from the calibrated data for each instrument from inter-spacecraft comparisons, is that for magnetic fields with $|B| < 200$ nT the accuracy is typically in the range 0.1 – 0.2 nT, and for higher fields of $|B| > 200$ nT, the accuracy is of the order of 0.4 nT. So far cross-calibration results indicate that the discrepancy between FGM and EDI varies between -0.4% and 1.3% with no dependence on FGM range, EDI CRF mode or date/time, which would make it very difficult to apply corrections to individual FGM field components on a consistent basis.

Intrinsic properties of the data and the quality of suitable data available for calibration both influence the quality of calibration that is achievable. Orbits for which the calibration quality falls outside of predefined limits are indicated by the presence of a caveat file in the CAA.

A time history of the over 200 calibration parameters is available, covering all ranges of the instruments on each of the four spacecraft. An initial survey of these statistics has been conducted from February 2001 to February 2012, demonstrating the overall stability or the parameters.

7. References

[1] Alconcel, L. N. S., P. Fox, P. Brown, T.M. Oddy, E. L. Lucek and C.M. Carr, *An initial investigation of the long-term trends in the fluxgate magnetometer (FGM) calibration parameters on the four Cluster spacecraft*, Geosci. Instrum. Method. Data Syst. Discuss., 4, 43-84, doi:10.5194/gid-4-43-2014,2014.

[2] Carr, C., P. Brown, L.-N. Alconcel, P. Brown, T. Oddy, P. Fox *User Guide to the FGM measurements in the Cluster ActiveArchive,* 30/10/2015. (http://caa.estec.esa.int/caa/ug_cr_icd.xml)

[3] Balogh et al., *The Cluster Magnetic Field Investigation*, Space Science Reviews, Vol. 79, No. 1-2, 01/1997

[4] Balogh et al., *The Cluster magnetic field investigation: overview of in-flight performance and initial results*, Annales Geophysicae, Vol. 19, pp. 1207-1217, 2001.

[5] Hedgecock, P. C.: A correlation technique for magnetometer zero level determination, Space Sci. Inst., 1, 83-90 (1975)

[6] Carr et al., *Cluster Active Archive: Interface Control Document for FGM*, 30/10/2015. (http://caa.estec.esa.int/caa/ug_cr_icd.xml

[7] Carr et al., *FGM report to the Cluster Active Archive Operation Review 2015*, 30/10 (http://caa.estec.esa.int/caa/reviews.xml)

[8] Gloag J. M., E. A. Lucek, L.–N. Alconcel, A. Balogh, P. Brown, C. M. Carr, C. N. Dunford, T. Oddy, J. Soucek, FGM data products in the CAA, in *The Cluster Active Archive - Studying the Earth's Space Plasma Environment,* edited by H. Laakso, M.G.G.T. Taylor, C.P. Escoubet, Springer, 2010.

[9] Kepko E. L., K. K. Khurana, M. G. Kivelson, R. C. Elphic and C. T. Russell, *Accurate determination of magnetic field gradients from four point vector measurements: 1. Use of natural constraints on vector data obtained from a single spinning spacecraft*, IEEE Trans. Magn., Vol. 32, p. 377, 1996.

[10] Khurana K. K., E. L. Kepko, M. G. Kivelson and R. C. Elphic, *Accurate determination of magnetic field gradients from four-point vector measurements: 2. Use of natural constraints on vector data obtained from four spinning spacecraft*, IEEE Trans. Magn., vol. 32, No. 5, p. 5193, 1996.

[11] P. Robert, C. Burlaud and M. Maksimovic*, Calibration report of STAFF Measurements in the Cluster Active Archive (CAA)*. (http://caa.estec.esa.int/caa/ug_cr_icd.xml)

[12] K. Nykyri et al. *Origin of the turbulent spectra in the high-altitude cusp: Cluster spacecraft observations*, Ann. Geophys., 24, 1057-1075, 2006